Archives of Acoustics Vol. ***, No. ***, https://doi.org/10.24423/archacoust.2026.4514

Online First October 7, 2026

Research Paper

Speed-Confounded Before–After Assessment of Tramway Pass-By Noise Under Track-Renewal Field Conditions

Tomasz Nowakowski*, Jacek Dwornik, Michał Strzelczyk

Poznan University of Technology
Poznań, Poland

*Corresponding Author: tomasz.nowakowski@put.poznan.pl

Received May 25, 2026; accepted June 3, 2026;
available online June 9, 2026; version of record October 7, 2026; published issue XXXX.

This study investigates the system-level acoustic response of the tramway track renewal under real urban operating conditions, with emphasis on the confounding role of operating speed in before–after comparisons. Pass-by noise measurements were conducted on a tram route in Poznań before (2022) and after (2025) renewal, when a conventional ballasted track was replaced by a ballastless system. During the same period, the mean pass-by speed increased from 25.9 km/h to 58.1 km/h. Energetic, psychoacoustic, and spectral indicators were analysed using direct comparisons, quartile-based speed sensitivities, and an integrated year–speed–tram type regression model. The direct comparison showed an increase in L_{Aeq} of +3.37 dB, while SEL remained nearly unchanged ($\Delta \approx -0.06$ dB), indicating that higher instantaneous levels were largely offset by shorter pass-by durations. Spectral analysis revealed lower measured levels of approximately 4 dB to 11 dB in the 125 Hz to 200 Hz range and localised increases of up to 7 dB to 11 dB around 1.6 kHz to 2 kHz. Quartile-based per-km/h derivatives indicated lower 2025 local sensitivities for L_{Aeq}, SEL, and loudness N in the pooled dataset. However, speed-doubling sensitivities showed that this apparent flattening was partly scale-dependent and not uniform across quantiles. The integrated model provided supportive evidence for changed metric–speed relationships, particularly for L_{Aeq}, although common-reference slope estimates were partly extrapolative because of limited speed overlap. The results demonstrate the usefulness of speed-sensitive analysis for interpreting before–after tramway noise measurements under changing operating regimes and should be regarded as system-level field-condition responses rather than isolated causal effects of track renewal.

Keywords: rolling noise, tramway noise, track renewal, spectral analysis, psychoacoustics, sound exposure level.



Copyright © 2026 The Author(s).
This work is licensed under the Creative Commons Attribution 4.0 International CC BY 4.0 (https://creativecommons.org/licenses/by/4.0/).

1. Introduction

Tramway systems are widely promoted as sustainable urban transport solutions, but their acoustic impact remains a significant constraint in densely populated areas (International Association of Public Transport [UITP], 2019; Zhang *et al.*, 2026). Environmental noise is among the most frequently reported sources of nuisance and, in some countries, represents the dominant category of environmental complaints (City of Poznań, 2022), highlighting the growing importance of acoustics in the planning and modernisation of transport infrastructure. The dominant mechanism of external noise generation in tramway systems is rolling noise, which arises from vibrations excited at the wheel–rail contact due to surface roughness (Remington, 1976; Thompson, 2009). The wavelengths of geometric irregularities are mapped onto excitation frequencies that depend on vehicle speed; consequently, increasing speed generally leads to higher emission levels and a shift of spectral energy toward higher frequencies (Thompson, Jones, 2000). In practice, infrastructure renewal is often accompanied by changes in permitted operating speed resulting from improved geometric and dynamic properties of the track. Under such conditions,

separating the acoustic response of the track–vehicle system associated with infrastructure modifications from operational changes becomes challenging. In field measurements conducted during normal line operation, wheel and rail roughness contributions cannot usually be measured separately according to standardised procedures such as European Standard (2019). Therefore, renewal studies typically take the form of passive diagnostic experiments, where the acoustic signal recorded at a receiver point is analysed under real operating conditions. Previous tram-noise studies have used pass-by measurements, noise maps, and spectral analysis to identify dominant noise components and to support the development of passive attenuation concepts (Nowakowski *et al.*, 2019). Although this approach does not allow complete isolation of infrastructural variables, it provides valuable insight into the acoustic response of the track–vehicle system as experienced by residents (Nowakowski, Komorski, 2024). Speed plays a central role in this context. At lower speeds, traction noise may contribute significantly, while rolling noise above approximately 30 km/h becomes the dominant mechanism (Thompson, 2009). Changes in speed therefore influence not only energetic indicators such as L_{Aeq} and SEL but also the spectral structure of the signal, which complicates direct comparisons between measurement campaigns conducted before and after infrastructure renewal (International Organization for Standardization [ISO], 2013).

Beyond energetic measures, psychoacoustic indicators such as loudness, sharpness, and psychoacoustic roughness are increasingly applied in environmental noise studies because they correlate more closely with perceived annoyance (Nowakowski, Komorski, 2024). Previous research has also shown that residents' responses to changes in transport infrastructure may be nonlinear, exhibiting both an excess response and an under-response relative to classical exposure–response relationships (Tetsuya *et al.*, 2017). This suggests that the acoustic impact of infrastructure renewal should be evaluated not only in terms of changes in sound levels, but also in terms of spectral and perceptual characteristics. Despite extensive research on rolling noise mechanisms and track construction, the interpretation of before–after measurements remains challenging when operating conditions change simultaneously with infrastructure. In particular, increases in operating speed after modernisation may lead to higher instantaneous energetic and psychoacoustic indicators, even if the structural behaviour of the track–vehicle system has improved.

The existing literature rarely addresses this problem by explicitly analysing the sensitivity of acoustic indicators to operating speed in before–after studies. This study therefore proposes a speed-adjusted assessment framework in which the track–vehicle–operation system response is evaluated using the sensitivity of acoustic metrics to speed ($\partial Y/\partial V$) within empirically observed speed ranges. In particular, sensitivities are evaluated in the lower and upper quartiles of the speed distribution (Q25 and Q75), enabling a comparison of acoustic behaviour under representative operating regimes without the need for extrapolation beyond the range of measured data.

The proposed framework is applied to a field study on tram track renewal in Poznań, where measurements carried out before and after modernisation were accompanied by a substantial increase in operating speed. By analysing energetic, spectral, and psychoacoustic indicators together with their speed sensitivities, the study aims to provide a more robust interpretation of before–after measurements under realistic operating conditions.

2. Objects of the study

The object of the study was the tram track structure on the Kornicka route in Poznań, analysed before and after the renewal. The pre-renewal configuration (representative for the 2022 campaign, based on available archival information) was a conventional ballasted track with grooved rails mounted on steel baseplates and supported by reinforced-concrete sleepers of the Ps type. The ballast consisted of crushed stone (originally filled up to the rail head level) underlain by a sand layer of approximately 0.07 m. A simplified schematic comparison is provided in Fig. 1. The renewed track section consisted of a ballastless system with prestressed concrete sleepers mounted on a polyurethane levelling layer and a reinforced concrete strip foundation (C30/37), supported by cement-bound and unbound subgrade layers. Based on its design, the renewed ballastless structure may be expected to modify the dynamic support conditions compared with the former ballasted track. However, no direct measurements of dynamic stiffness, track decay rate, admittance, or transfer functions were performed; therefore, spectral interpretations are treated as physically plausible explanations rather than directly verified mechanisms.

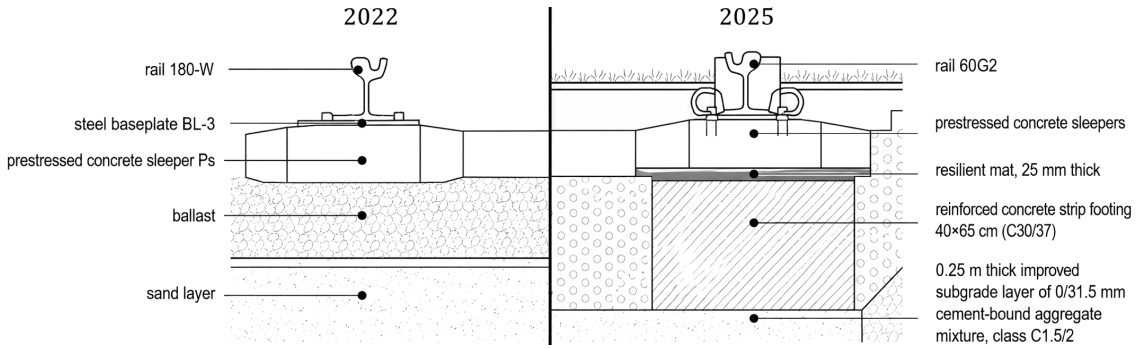


Fig. 1. Simplified schematic of the tram track structure, showing the pre-renewal configuration representative for the 2022 campaign (left) and the post-renewal configuration representative for the 2025 campaign (right).

During both campaigns, three tram types in regular operation in Poznań were included (Fig. 2). Type A was the Moderus Gamma, a three-section fully low-floor tram approximately 31.5 m to 32.0 m long, with an empty mass of about 40 t to 43 t and all axles powered. Type B was the Solaris Tramino S105p, a five-section fully low-floor tram approximately 32 m long and 40 t to 41 t in empty mass, with two powered bogies and one non-powered bogie. Type C was the Moderus Beta, a three-section partially low-floor tram approximately 28.0 m to 28.5 m long and 36 t to 38 t in empty mass, with two powered bogies. The installed traction power was approximately 400 kW for types A and B and approximately 240 kW to 300 kW for type C, depending on the subseries. These differences justified treating tram type as a broad rolling-stock class in the analysis.

Type A: Moderus Gamma



Type B: Solaris Tramino S105p



Type C: Moderus Beta



Fig. 2. Tram types included in the pass-by measurements (photos: Michał Strzelczyk).

3. Methods and measurement conditions

The pass-by tram noise measurements were conducted in Poznań (Poland) on the Kornicka Route. The investigated straight track section is approximately 2 km long and was measured in two campaigns, in September 2022 (pre-renewal) and in August 2025 (post-renewal). The measurement site is located in an urban residential area between two buildings. A vegetation strip (height ≤5 m) and a grass strip (width ≈6 m) separate the buildings from the track. A bicycle path and a pedestrian walkway are present on the southern side of the track. Only tram pass-bys on the northern track (marked in blue in Fig. 3) were included in the analysis.

The microphone position was established according to (ISO, 2013). The microphone was placed at a distance of 7.5 m from the track centreline (±0.8 m). The microphone height was set to 1.2 m (±0.05 m). A photoelectric gate (photocell) was used to detect the leading and trailing edges of each vehicle, enabling time-window selection of the acoustic signal corresponding to the interval in which the tram occupied the measurement cross section. A B&K 4189 measurement microphone with a B&K 2671 preamplifier was used. The microphone sensitivity was 49.3 mV/Pa (uncertainty at the 95 % confidence level, 0.2 dB). The frequency range was 6.3 Hz to 20 kHz, the dynamic range was 14.6 dB to 146 dB, the operating temperature range was −30 °C to +150 °C, and the microphone was prepolarized. Data acquisition was performed using a six-channel B&K LAN-XI 3050-A-60 module. The sampling frequency during the measurements was 65 536 Hz.



FIG. 3. Pass-by noise measurement point: 2022 campaign (left) and 2025 campaign (centre) photos by the authors; satellite view (right) from the OpenAerialMap viewer (OpenAerialMap, 2026).

Stable weather conditions were observed during both measurement campaigns. In September 2022, the recorded temperatures were 15 °C to 23 °C, relative humidity 45 % to 70%, atmospheric pressure 1010 hPa to 1025 hPa, and wind speed typically 2 m to 5 m/s. In August 2025, warmer conditions were observed, with temperature 22 °C to 30°C, relative humidity 40 % to 65%, atmospheric pressure 1008 hPa to 1020 hPa and wind speed 2 m/s to 6 m/s. Measurement results are reported together with an uncertainty estimated using a budget approach, considering only type B contributions (standard uncertainties u_i in dB, 1σ), with independent components and rectangular distributions for tolerances ($u = a/\sqrt{3}$) (Joint Committee for Guides in Metrology [JCGM], 2008; CRAVEN, KERRY, 2007). The microphone distance tolerance was converted into an equivalent level contribution using free-field spreading and included as u_{dist} (ISO 2013; CRAVEN, KERRY, 2007). Measurement geometry and quality control followed ISO (2013). For both the 2022 and 2025 campaigns, the type B components (in dB) were as follows, meteorology (0.58), distance (0.537), microphone (0.10), calibrator (0.09), preamplifier (0.02), power supply (0.03), and windscreen (0.03). The combined standard uncertainty was $u_c = 0.803$ dB (RSS) and the expanded uncertainty (95 %, $k = 2$) was $U = 1.616$ dB, i.e., results can be reported as $x \pm 1.6$ dB.

Wheel–rail surface roughness was not measured in accordance with European Standard (2019). This limits causal interpretation because roughness directly affects rolling-noise excitation and may change over time due to wear, maintenance, and wheel reprofiling. Consequently, the measured pass-by noise is interpreted as the effective system-level response of the combined track–vehicle–operation system. Using the same rolling-stock classes in both campaigns reduces, but does not eliminate, vehicle-related variability.

To analyse the dependence of acoustic indicators on pass-by speed (V), linear, quadratic, cubic, logarithmic, power-law, and exponential models were compared using $\mathrm{AIC_c}$. When competing models differed by less than 2 $\mathrm{AIC_c}$ units, the simpler model was selected. The model adequacy was checked using the LOOCV RMSE and repeated train/test RMSE; for subsets with $n < 30$, an additional no-cubic sensitivity check was performed to assess potential overfitting.

Speed sensitivity was defined as the local derivative $\partial Y/\partial V$ of the selected parsimonious model and evaluated at Q25, Q50, and Q75 of the observed speed distribution within each subset. The primary interpretation used Q25 and Q75 as representative in-range regimes, with uncertainty quantified using 1000-iteration nonparametric bootstrap resampling. Because the speed ranges differed strongly between campaigns, sensitivities were interpreted within each year's empirical speed range rather than as direct same-speed contrasts.

To reduce scale effects caused by the different speed ranges, local sensitivities were also expressed with respect to log-speed and speed doubling:

$$S_{\log_{10}} = \frac{dY}{d\log_{10}(V)} = \ln(10)\, V \frac{dY}{dV}, \qquad S_{2\times} = \ln(2)\, V \frac{dY}{dV}, \tag{1}$$

where V is expressed in km/h, and $S_{2\times}$ represents the local change associated with speed doubling. These quantities and their bootstrap confidence intervals were obtained by applying the same transformations to the corresponding dY/dV estimates at Q25, Q50, and Q75.

For each energetic and psychoacoustic metric, an integrated regression model was fitted to assess whether the metric–speed relationship differed between campaigns after adjustment for the tram type. The year was coded as a binary 2025 indicator, the tram type as a categorical fixed effect, and the speed as the mean-centred V_c. Because speed ranges differed strongly between years, the year main effect was not interpreted as a direct cause-and-effect contrast at the same speed. The linear specification was defined as

$$y_i = \beta_0 + \beta_1 I(\text{Year}_i = 2025) + \beta_2 V_{c,i} + \beta_3 I(\text{Year}_i = 2025) \cdot V_{c,i} + \gamma_{\text{tram}(i)} + \varepsilon_i, \tag{2}$$

where y_i is the acoustic or psychoacoustic metric, $V_{c,i}$ is mean-centred speed, $\gamma_{\text{tram}(i)}$ is the tram-type fixed effect, and ε_i is the residual error.

A spline alternative replaced V_c with a cubic regression spline basis $f(V_c)$ with $df = 3$, including the analogous year × spline interaction:

$$y_i = \beta_0 + \beta_1 I(\text{Year}_i = 2025) + f(V_{c,i}) + I(\text{Year}_i = 2025) \cdot f(V_{c,i}) + \gamma_{\text{tram}(i)} + \varepsilon_i. \tag{3}$$

Linear and spline specifications were compared using AIC_c. The spline model was selected only when its AIC_c was more than 2 units lower than that of the linear model; otherwise, the linear model was retained. Models were fitted using OLS, and inference used HC3 robust standard errors with joint Wald tests for year, speed, year × speed, and tram-type effects. The Benjamini–Hochberg FDR correction was applied to the year and year × speed terms across metrics. Because the 2022 and 2025 speed ranges were largely non-overlapping, interaction effects and local slope contrasts from the integrated model were interpreted as adjusted field-condition associations rather than causal estimates of the isolated track renewal effect.

The study focused on exterior pass-by noise at the ISO (2013) receiver position, representing a near-track pedestrian receiver rather than a facade exposure point. Signal post-processing and indicator computation were performed in B&K Connect for the same pass-by event windows. The reported psychoacoustic indicators are therefore interpreted as receiver-side descriptors of the measured tram pass-by signal, not as direct annoyance or listening-test outcomes. Indicator definitions and calculation settings are summarised in Table 1.

Table 1. Acoustic and psychoacoustic indicators calculated in B&K Connect and used in the study.

Full name	Symbol	Unit	B&K Connect calculation settings
A-weighted equivalent sound pressure level	L_{Aeq}	dB	Standard energetic acoustic indicator
Sound exposure level	SEL	dB	SEL = $L_{\text{Aeq}} + 10\log_{10}\left(\frac{T_p}{T_0}\right)$, where T_p is the pass-by duration and $T_0 = 1$ s.
Articulation index	AI	%	Beranek articulation index (Kryter, 1962).
Loudness	N	sone	Sound field: free; ISO (2017), Zwicker time-varying loudness method (ISO, 2017).
Sharpness	S	acum	Zwicker sharpness method; B&K implementation according to sound quality metrics workflow (ISO, 2017).
Fluctuation strength	FS	vacil	Default modulation frequency: 4 Hz; Zwicker and Fastl sound quality metric (ISO, 2017).
Roughness	R	asper	Default modulation frequency: 70 Hz; Zwicker and Fastl sound quality metric (ISO, 2017).
Tone-to-noise ratio	TNR	dB	Frequency resolution: 2 Hz; tone threshold: 1 dB; maximum number of tones: 5; maximum tone width: 15 %; tone detection: discrete; ANSI S1.13:2005; B&K tonal metrics implementation (American National Standards Institute, 2025).
Prominence ratio	PR	dB	Discrete tone detection; ANSI S1.13:2005; also consistent with tonal prominence approaches used in ECMA-74 and ISO 7779 (American National Standards Institute, 2025).
Tonal-component level	L_T	dB	ANSI S1.13:2005 tonal metrics workflow (American National Standards Institute, 2025).
Tonality	T	–	Terhardt pitch-salience / tonality method (Terhardt *et al.*, 1982).

4. Results

4.1. Rolling-stock composition and operating speed

A comparative analysis was performed of (a) the rolling-stock composition and (b) the tram pass-by speed distributions for the 2022 and 2025 measurement campaigns. The analysis included a $\chi 2$ test for contingency tables, assessment of speed-distribution shape and variance (normality tests and Levene's test), and between-group comparisons (nonparametric tests and a bootstrap estimate of the median-speed difference). The results are summarised in Fig. 4.

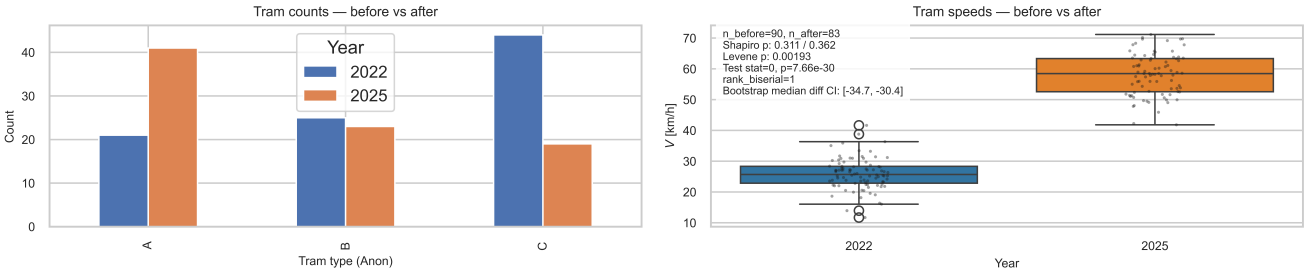


Fig. 4. Summary of rolling-stock composition and tram pass-by speed distributions for the 2022 and 2025 measurement campaigns.

The results in Fig. 4 indicate substantial changes in both the rolling-stock mix and the pass-by speed distribution between 2022 and 2025. The vehicle-type counts were as follows: type A – 21 (2022) vs 41 (2025), type B – 25 vs 23, and type C – 44 vs 19. The $\chi 2$ test confirmed a statistically significant change in composition ($\chi 2 = 16.199$, $df = 2$, $p = 0.0003$). The authors had no influence on which trams operated on the line or on their operating conditions (including speeds) during the measurement periods.

The speed analysis indicates that in 2022 ($n = 90$) the mean speed was 25.90 km/h (median 25.69 km/h, SD = 5.04 km/h), whereas in 2025 ($n = 83$) the mean increased to 58.09 km/h (median 58.46 km/h, SD = 6.76 km/h). Diagnostic tests did not indicate substantial deviations from normality; however, unequal variances were observed. Therefore, the nonparametric Mann–Whitney test was applied and indicated an extremely significant difference ($U = 0$, $p \approx 7.7 \times 10^{-30}$). The effect size (rank-biserial correlation ≈ 1.0) and the bootstrap confidence interval for the median difference (−34.71 km/h to −30.40 km/h; difference computed as 2022–2025) indicate a very large and practically relevant increase in speed of approximately 30 km/h to 35 km/h in 2025 relative to 2022. Therefore, a direct comparison of average acoustic levels would be misleading.

4.2. Direct comparison of acoustic indicators

Mean values of energetic and psychoacoustic indicators were compared between campaigns for the pooled dataset and tram types A–C (Table 2, Fig. 5). Differences were expressed as $\Delta = 2025 - 2022$; percentage changes were reported only for non-decibel indicators. SEL was derived from L_{Aeq} and pass-by duration.

The expanded measurement uncertainty ($U = 1.61$ dB) characterizes the uncertainty of individual sound level estimates under the assumed measurement budget. It should not be interpreted as the only uncertainty of before–after differences, because these differences also include pass-by variability, speed variability, rolling-stock variability, and model uncertainty. Therefore, unadjusted differences smaller than or comparable to U, such as the pooled SEL difference of approximately −0.06 dB, are not interpreted as acoustically meaningful. Larger descriptive differences, such as the pooled L_{Aeq} increase of +3.37 dB, exceed the measurement uncertainty but remain confounded by the substantial change in operating speed.

4.3. Speed-dependent modelling of L_{Aeq}, SEL, and loudness N

The dependence of the three main indicators, L_{Aeq}, SEL, and loudness N, on the tram pass-by speed V was analysed separately for tram types A–C and for the pooled dataset. The candidate models were compared

TABLE 2. Direct comparison of acoustic and psychoacoustic indicators between the 2022 and 2025 campaigns.

Metric	All				Type A		Type B		Type C	
	2022	2025	Δ	%	Δ	%	Δ	%	Δ	%
FS [vacil]	0.919	1.703	0.784	85.3	0.797	87.2	0.833	100.5	0.763	78.4
L_{Aeq} [dB]	74.22	77.59	3.37	–	1.55	–	5.26	–	3.44	–
SEL [dB]	80.52	80.47	−0.06	–	−1.93	–	1.68	–	−0.07	–
N [sone]	44.72	53.51	8.79	19.6	5.78	12.3	10.73	24.4	9.57	21.7
PR [dB]	5.99	8.31	2.32	–	4.44	–	0.93	–	−0.56	–
R [asper]	1.359	1.261	−0.098	−7.2	−0.096	−7.1	−0.034	−2.6	−0.129	−9.3
S [acum]	1.272	1.429	0.158	12.4	0.179	14.1	0.172	13.7	0.105	8.2
T [–]	0.050	0.082	0.033	65.6	0.045	95.2	0.026	43.0	0.009	20.1
L_T [dB]	71.05	71.76	0.70	–	−1.03	–	−1.35	–	4.57	–
TNR [dB]	−5.45	−1.96	3.48	–	3.01	–	2.33	–	5.57	–

Note: Δ = 2025 – 2022. Percentage changes are reported only for non-decibel indicators.

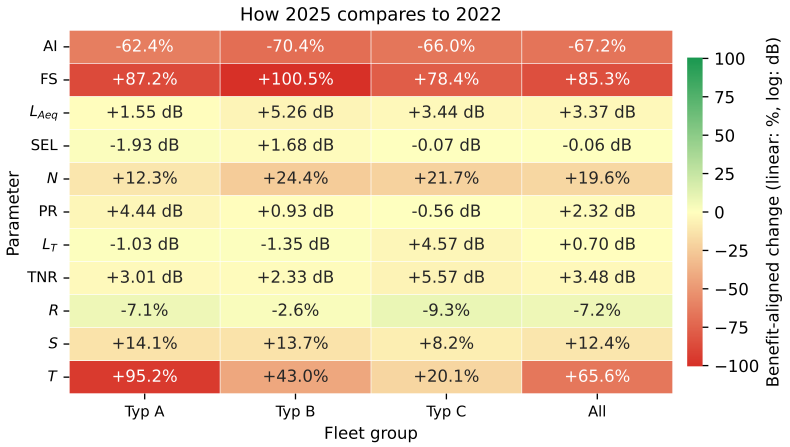


FIG. 5. Heatmap summary of direct before–after changes in acoustic and psychoacoustic indicators.

using the $\mathrm{AIC_c}$, and the predictive stability was checked using the LOOCV and repeated train/test RMSE. The selected parsimonious models are reported in Table 3 to Table 5. For small subsets ($n < 30$), the robustness of the selected model was verified using a restricted candidate set excluding cubic models. Sensitivity was defined as the local derivative $\frac{dY}{dV}$ of the selected model with respect to speed and was evaluated only within empirically observed speed ranges, at Q25 and Q75 of the speed distribution. Slopes are expressed in dB/(km/h) for L_{Aeq} and SEL, and in sone/(km/h) for loudness N.

TABLE 3. Parsimonious $\mathrm{AIC_c}$-selected models for $L_{\mathrm{Aeq}}(V)$ and corresponding local speed sensitivities evaluated at Q25 and Q75.

Group	Year	n	Selected model	$\mathrm{AIC_c}$	LOOCV RMSE	Q25 slope [dB/(km/h)]	Q75 slope [dB/(km/h)]
A	2022	21	quadratic	−21.44	0.57	0.806	0.431
A	2025	41	exponential	24.83	1.36	0.301	0.312
B	2022	25	cubic	−24.74	0.94	0.553	0.591
B	2025	23	exponential	12.74	1.29	0.370	0.392
C	2022	44	cubic	35.87	1.81	0.700	0.956
C	2025	19	exponential	12.88	1.35	0.357	0.371
all	2022	90	exponential	80.60	1.59	0.623	0.654
all	2025	83	quadratic	60.98	1.43	0.267	0.434

As a scale-normalised complement to the per-km/h derivatives, local sensitivities were also expressed per speed doubling, $S_{2\times}$. In the pooled dataset, this analysis produced a non-uniform between-year pattern: for L_{Aeq} and SEL, $S_{2\times}$ was slightly lower at Q25 but higher at Q50 and Q75 in 2025, whereas for loudness N, $S_{2\times}$ was higher

TABLE 4. Parsimonious AIC_c-selected models for SEL(V) and corresponding local speed sensitivities evaluated at Q25 and Q75.

Group	Year	n	Selected model	AIC_c	LOOCV RMSE	Q25 slope [dB/(km/h)]	Q75 slope [dB/(km/h)]
A	2022	21	quadratic	−21.38	0.57	0.623	0.275
A	2025	41	exponential	25.50	1.37	0.228	0.235
B	2022	25	cubic	−24.55	0.97	0.368	0.449
B	2025	23	exponential	13.46	1.31	0.298	0.312
C	2022	44	cubic	35.98	1.81	0.507	0.801
C	2025	19	exponential	13.09	1.37	0.280	0.288
all	2022	90	exponential	82.28	1.60	0.464	0.479
all	2025	83	quadratic	56.43	1.40	0.188	0.373

TABLE 5. Parsimonious AIC_c-selected models for loudness $N(V)$ and corresponding local speed sensitivities evaluated at Q25 and Q75.

Group	Year	n	Selected model	AIC_c	LOOCV RMSE	Q25 slope [sone/(km/h)]	Q75 slope [sone/(km/h)]
A	2022	21	linear	−1.91	0.93	1.343	1.343
A	2025	41	linear	77.14	2.55	0.676	0.676
B	2022	25	linear	44.79	2.40	1.142	1.142
B	2025	23	exponential	45.54	2.64	0.667	0.783
C	2022	44	cubic	75.10	2.63	1.128	1.620
C	2025	19	exponential	50.88	3.71	0.709	0.798
all	2022	90	exponential	176.75	2.72	1.089	1.260
all	2025	83	exponential	178.60	2.92	0.644	0.741

at all evaluated quantiles. Thus, the lower values of $\frac{dY}{dV}$ in 2025 should not be interpreted as direct evidence of a uniformly flatter acoustic response, because part of the apparent flattening reflects the speed-scale dependence under substantially different operating-speed regimes. A pooled summary of the speed-doubling sensitivities is provided in Table A1 in Appendix.

The pooled models showed lower per-km/h local sensitivities in 2025 for all three main indicators. For L_{Aeq}, SEL, and N, the Q25/Q75 sensitivities decreased respectively from 0.623–0.654 to 0.267–0.434 dB/(km/h), from 0.464–0.479 to 0.188–0.373 dB/(km/h), and from 1.089–1.260 to 0.644–0.741 sone/(km/h). However, because the speed-doubling analysis did not show a uniformly lower 2025 response, these per-km/h derivatives are interpreted as local, regime-specific sensitivities rather than evidence of a uniformly flatter acoustic response. Type-specific patterns were more variable and are treated as exploratory because of smaller subgroup sizes and the uncontrolled vehicle condition. The restricted no-cubic check for small subsets did not alter the qualitative pooled interpretation. The corresponding quartile-based local sensitivities for L_{Aeq}, SEL, and loudness N are visualised in Fig. 6.

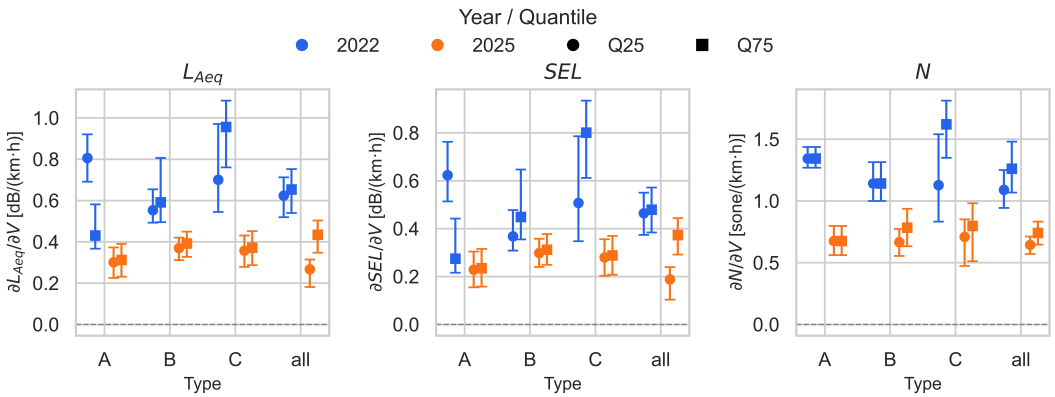


FIG. 6. Quartile-based local speed sensitivities for L_{Aeq}, SEL, and loudness N, evaluated at Q25 and Q75 within the observed speed ranges.

A broader summary of speed-adjusted sensitivity changes across all analysed metrics and tram types is shown in Fig. 7.



FIG. 7. Speed-adjusted sensitivity summary across metrics and tram types at low-speed (Q25) and high-speed (Q75) operating regimes.

4.4. Spectral analysis (Bark and 1/3-octave bands)

To contextualize the previously reported changes in energetic and psychoacoustic indicators and to identify spectral regions associated with these differences, a frequency-domain analysis was performed in two complementary representations: the Bark scale, corresponding to critical bands (Fig. 8), and conventional 1/3-octave bands (Fig. 9). For each measurement campaign (2022 and 2025), band-wise energy matrices were extracted. The spectra were then averaged separately for each rolling-stock class and year to obtain representative characteristics, and the level difference was computed as $\Delta L = L_{2025} - L_{2022}$.

In the Bark representation, the 2025 curves are generally lower than the 2022 curves in the lowest Bark bands (approximately Bark 1.5–3.0), which indicates lower measured low-frequency components for the 2025 dataset. The magnitude of this difference depends on the tram type. Above approximately Bark 10, the spectra intersect and the 2025 levels become locally higher than in 2022, indicating that the between-campaign change was not a uniform broadband reduction, but rather a frequency-dependent redistribution of the measured acoustic energy.

The 1/3-octave-band spectra provide a conventional view of the same redistribution. In the 2025 campaign, lower measured levels were observed in the 125 Hz to 200 Hz range, with differences of approximately 4 dB to 11 dB depending on the tram type. At the same time, local increases occurred in the mid-frequency range around 1.6 kHz to 2 kHz, reaching approximately +7 dB to +11 dB in selected tram-type comparisons. These spectral differences should not be interpreted as an isolated effect of the track structure, because operating speed increased substantially between campaigns and wheel–rail roughness was not measured.

The heatmaps (Fig. 10) provide a compact view of the same frequency-dependent redistribution. In the Bark representation, lower post-renewal values are visible in the low-Bark region, while a localised increase appears around Bark 11.5–12.5. In the 1/3-octave representation, the main lower-level region occurs around 125 Hz to 200 Hz, whereas local increases are visible around 1.6 kHz to 2 kHz. These regions are potentially

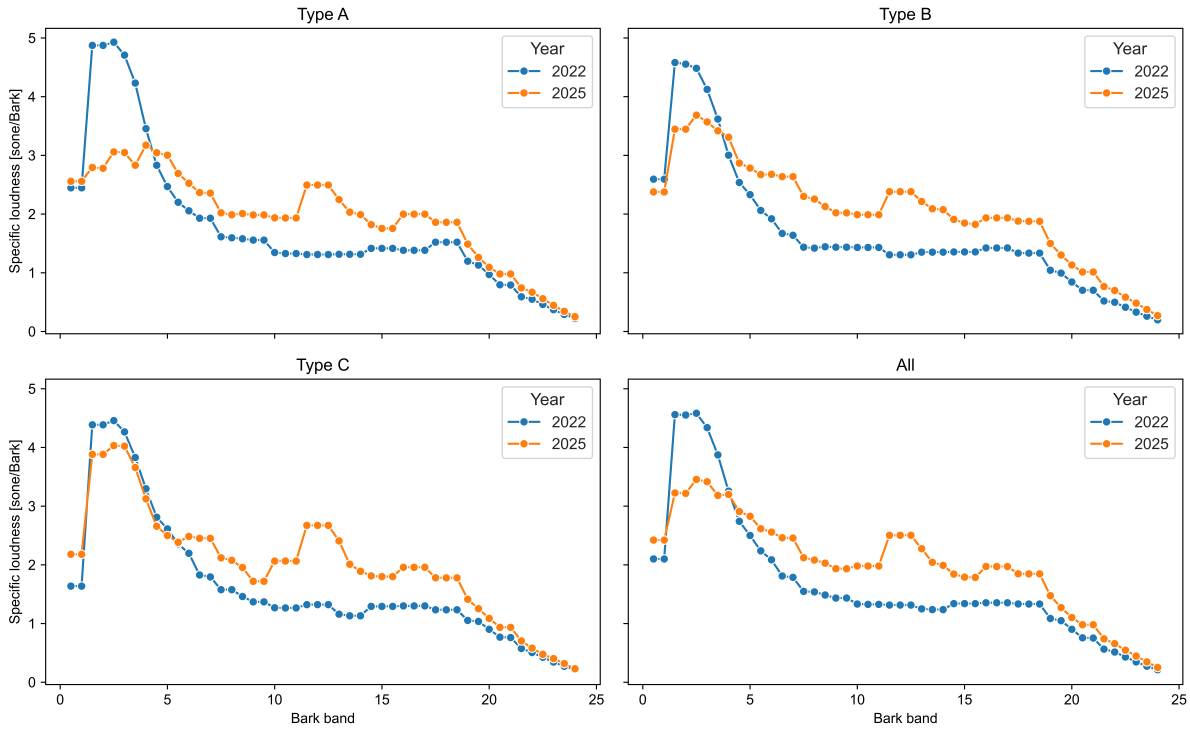


FIG. 8. Average Bark-scale spectra by tram type for the 2022 and 2025 measurement campaigns. The curves represent measured receiver-side spectral characteristics under the operating conditions present in each campaign.

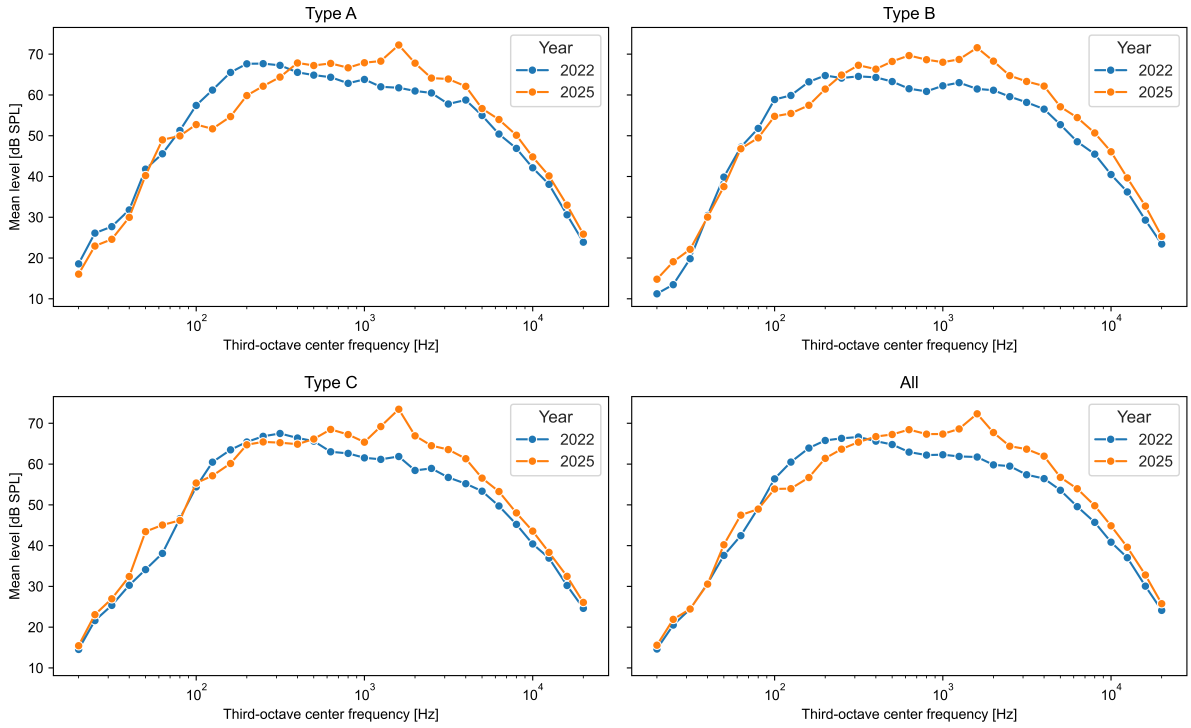


FIG. 9. Average 1/3-octave-band SPL spectra by tram type for the 2022 and 2025 measurement campaigns. Differences between campaigns should be interpreted together with the change in operating speed and the absence of direct wheel–rail roughness measurements.

relevant to perceived low-frequency character and to mid-frequency sharpness or tonality-related attributes, respectively; however, their perceptual interpretation remains indirect because no dedicated listening test or annoyance assessment was performed in the present study.

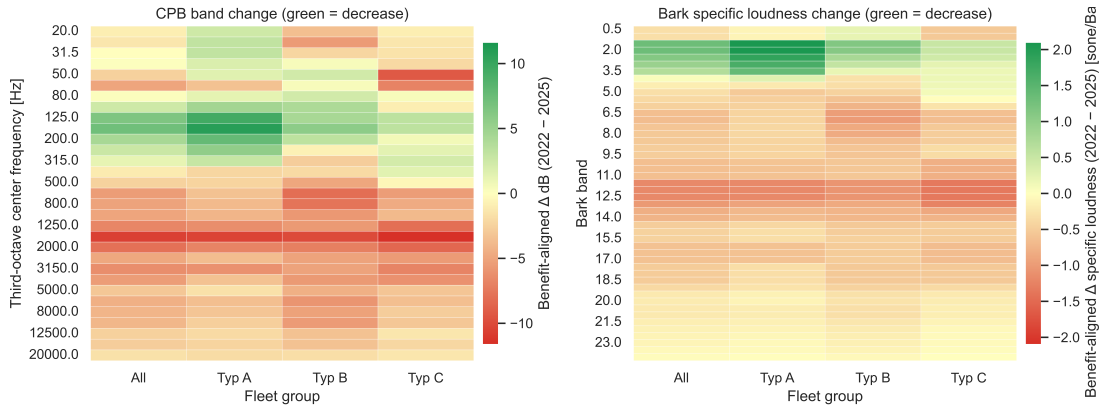


FIG. 10. Frequency-dependent redistribution between campaigns shown as heatmaps for 1/3-octave-band level changes and Bark-scale specific-loudness changes. Colours indicate post-renewal differences, with green denoting lower 2025 values and red denoting higher 2025 values.

Because excitation frequency scales with speed, fixed frequency bands do not correspond to fixed roughness wavelengths. Using $\lambda = V/f$, the 125 Hz to 200 Hz range corresponds to approximately 57.5 mm to 36.0 mm at 25.9 km/h and 129.1 mm to 80.7 mm at 58.1 km/h, whereas the 1.6 kHz to 2 kHz range corresponds to 4.5 mm to 3.6 mm and 10.1 mm to 8.1 mm, respectively (Table 6). Thus, part of the spectral redistribution may reflect speed-induced frequency mapping rather than changes in track radiation alone.

TABLE 6. Equivalent roughness wavelengths for selected frequency bands at the mean pass-by speeds measured in 2022 and 2025.

Frequency band [Hz]	λ [mm], V = 25.9 km/h	λ [mm], V = 58.1 km/h	Interpretation
125	57.5	129.1	Low-frequency reduction range
160	44.9	100.9	Low-frequency reduction range
200	36.0	80.7	Low-frequency reduction range
1600	4.5	10.1	Mid-frequency increase range
2000	3.6	8.1	Mid-frequency increase range

4.5. INTEGRATED YEAR–SPEED–TRAM TYPE MODEL

The integrated year–speed–tram type model assessed whether metric–speed relationships differed between campaigns after adjustment for the broad rolling-stock class. Linear and spline specifications were compared using the AIC_c, and inference was based on HC3 robust Wald tests with the Benjamini–Hochberg correction (Table 7).

TABLE 7. Integrated year–speed–tram type model summary. Values are AIC_c-based model-selection results and HC3 robust Wald-test p-values with Benjamini–Hochberg q-values for the year and year × speed terms.

Metric	Model	AIC_c lin.	AIC_c spl.	ΔAIC_c	p-year	p-speed	p-year × speed	p-tram type	q-year	q-year × speed
AI [%]	linear	890.75	893.63	2.87	<0.001	<0.001	<0.001	0.01	<0.001	<0.001
FS [vacil]	spline	26.50	4.02	−22.49	0.63	<0.001	0.02	<0.001	0.63	0.04
L_{Aeq} [dB]	linear	638.31	636.56	−1.75	<0.001	<0.001	<0.001	0.08	<0.001	<0.001
L_T [dB]	linear	882.88	888.34	5.46	0.12	<0.001	0.02	0.29	0.17	0.04
N [sone]	spline	848.22	845.12	−3.09	0.52	<0.001	0.05	0.03	0.57	0.08
PR [dB]	spline	765.36	749.49	−15.87	0.05	<0.001	0.11	<0.001	0.11	0.16
R [asper]	linear	−212.58	−209.06	3.52	0.48	<0.001	0.01	0.31	0.57	0.03
S [acum]	linear	−439.05	−430.80	8.25	<0.001	0.20	0.16	0.05	<0.001	0.19
SEL [dB]	spline	642.63	636.56	−6.06	0.12	<0.001	0.09	0.75	0.17	0.14
T [–]	spline	−863.15	−867.59	−4.44	0.12	0.52	0.25	<0.001	0.17	0.28
TNR [dB]	linear	791.84	797.16	5.32	<0.001	0.37	0.42	0.36	<0.001	0.42

Note: n = 173. $\Delta AIC_c = AIC_{c\,spl.} - AIC_{c\,lin.}$. The spline model was selected only when its AICc was more than 2 units lower than that of the linear model ($\Delta AIC_c < -2$); otherwise, the linear model was retained. P-values are HC3 robust joint Wald tests.

After the FDR correction, between-year shifts were supported for L_{Aeq}, AI, S, and TNR, whereas year × speed interactions were supported for AI, L_{Aeq}, R, FS, and L_T. Because empirical speed ranges differed strongly, common-reference slope estimates were partly extrapolative. At the pooled median reference speed ($V \approx 35.9\,\mathrm{km/h}$), the reference point was within the 2022 range but below the 2025 range. Therefore, Fig. 11 is interpreted as supportive model-based evidence, while the primary interpretation relies on the in-range quartile sensitivities.

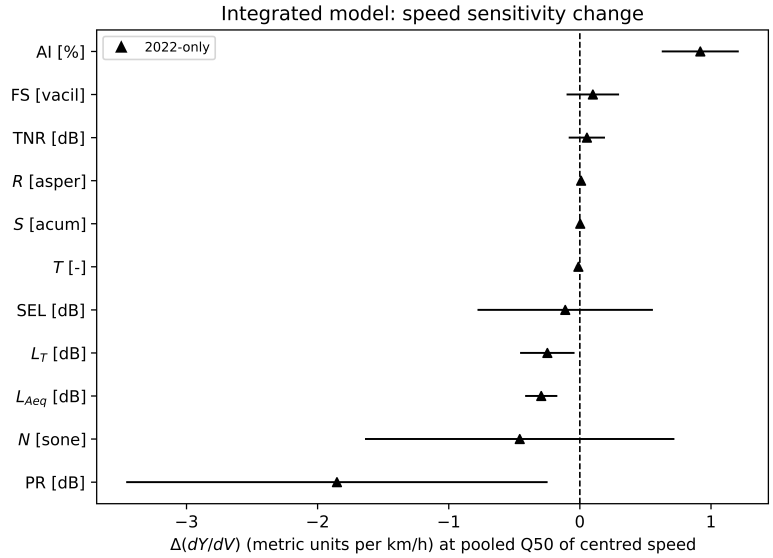


Fig. 11. Model-based change in local speed sensitivity from the integrated year–speed–tram type model. Points show $\Delta\left(\frac{dY}{dV}\right) = \left(\frac{dY}{dV}\right)_{2025} - \left(\frac{dY}{dV}\right)_{2022}$ (metric units per km/h) at pooled Q50(V_c), and horizontal bars show 95 % confidence intervals. Estimates are standardised over the tram type using pooled empirical A/B/C weights and should be interpreted as adjusted field-condition associations rather than an isolated causal effect of track renewal.

5. Discussion

The main confounder in this before–after comparison was the increase in mean pass-by speed from approximately 26 km/h to 58 km/h. For rolling noise, this affects both the emission level and the spectral distribution, because excitation frequencies scale with speed (Thompson, 2009). It may also change the dominant source composition: at the lower 2022 speeds, traction, gearbox, auxiliary, braking or acceleration-related components may have contributed more strongly, whereas at the 2025 speeds rolling noise is expected to dominate. The fleet composition and the individual vehicle condition provide additional confounding, since the number of observations within tram types differed between years and the vehicle-specific wheel condition was not controlled. Consequently, the results should be interpreted as system-level responses rather than purely infrastructure-driven changes.

A central outcome is the divergence between L_{Aeq} and SEL: in the pooled dataset, L_{Aeq} increased by +3.37 dB, whereas SEL remained practically unchanged ($\Delta \approx -0.06\,\mathrm{dB}$). This indicates that higher instantaneous levels were largely compensated by shorter pass-by durations and confirms that L_{Aeq} alone may be misleading in speed-confounded before–after comparisons.

The metric–speed modelling expressed in $\frac{dY}{dV}$ units indicates lower local per-km/h sensitivity in 2025 for the main pooled indicators within the reported in-range quartiles. However, because $\frac{dY}{dV}$ is expressed per 1 km/h, part of this reduction may reflect speed-scale dependence under substantially different operating-speed ranges. Scale-normalised sensitivities were therefore evaluated (Table A1 in Appendix). On this scale, the pooled 2025 response was not uniformly lower across quantiles. Thus, the apparent flattening in per-km/h derivatives should be interpreted as a local, regime-specific result rather than as direct evidence of a uniformly flatter acoustic response.

The spectral and psychoacoustic results indicate a frequency-dependent redistribution of receiver-side sound energy. Lower levels in the 125 Hz to 200 Hz range are consistent with changes in low-frequency track–vehicle behaviour, while increases around 1.6 kHz to 2 kHz correspond to rail-radiation-related rolling-noise components and help explain the observed increases in sharpness, tonality and loudness. Track support properties, including rail-pad stiffness and damping, can influence rolling-noise radiation and redistribute energy across frequency bands (Vincent *et al.*, 1996; Lakušić *et al.*, 2005; Sun *et al.*, 2020; Andrés *et al.*, 2022). This interpretation is consistent with earlier tram-track field measurements by Lakušić *et al.* (2005), who compared the double-elastic indirect DEPP system with the direct elastic ZG 3/2 system on a continuous concrete base and reported approximately 3 dB lower mean maximum pass-by noise for the DEPP site. They also showed that speeds below 20 km/h produced approximately 3 dB to 4 dB lower levels than speeds above 20 km/h, and that tram type affected the measured noise. These findings support the view that track support elasticity, rolling-stock class and operating speed jointly shape tram pass-by noise under field conditions. However, because wheel–rail roughness and track dynamic properties were not measured directly, this interpretation remains diagnostic and consistency-based rather than a unique identification of the source mechanism.

The study should not be interpreted as a strict causal attribution of the observed acoustic changes to infrastructure renewal alone. The measurements were conducted under real operating conditions, where infrastructure, speed, fleet composition, vehicle condition, wheel and rail condition, and maintenance history may change simultaneously. Wheel–rail surface roughness was not measured according to (European Standard, 2019), and no direct measurements of track decay rate, receptance, admittance, support stiffness or transfer functions were performed (Jones *et al.*, 2006). Consequently, the results describe a system-level field-condition response: lower local per-km/h sensitivities, lower measured low-frequency energy, higher relative energy around 1 kHz to 2 kHz, nearly unchanged SEL, and higher instantaneous L_{Aeq} under substantially higher operating speeds. The infrastructure and excitation-spectrum contributions cannot be fully separated.

6. Conclusions

This study evaluated tramway pass-by noise before and after track renewal under real urban operating conditions, focusing on system-level acoustic interpretation when operating speed differs substantially between campaigns.

The 2025 campaign was accompanied by a major increase in mean pass-by speed, from 25.9 km/h to 58.1 km/h. In the pooled dataset, L_{Aeq} increased by +3.37 dB, whereas SEL remained practically unchanged ($\Delta \approx -0.06$ dB), indicating that higher instantaneous levels were largely compensated by shorter pass-by durations. Thus, L_{Aeq} alone may be misleading in speed-confounded before–after assessments.

When speed was explicitly considered, per-km/h sensitivities ($\partial Y/\partial V$) were lower in 2025 for L_{Aeq}, SEL, and loudness N. However, speed-doubling sensitivities showed that this apparent flattening was partly scale-dependent and not uniform across quantiles. Therefore, dY/dV should be interpreted as a local, regime-specific derivative rather than direct evidence of a uniformly flatter acoustic response.

Spectral analysis showed redistribution rather than broadband reduction: lower measured levels in the 125 Hz to 200 Hz range and localised increases around 1.6 kHz to 2 kHz. The integrated year–speed–tram type model provided supportive adjusted evidence for changed metric–speed relationships, particularly for L_{Aeq}, but common-reference slope estimates were partly extrapolative because of the limited speed overlap.

Overall, the results demonstrate that substantial post-renewal speed changes can mask or distort direct before–after acoustic comparisons. The proposed quartile-based sensitivity framework provides a transferable way to interpret tramway noise measurements under changing operating regimes. The findings should be treated as a system-level field-condition comparison, not as an isolated causal estimate of the track renewal effect; causal separation would require wheel–rail surface roughness and direct track dynamic measurements.

Appendix

Table A1. Speed-doubling local sensitivities derived from in-range local derivatives (Q25, Q50, Q75). Values are expressed in metric units per speed doubling.

Metric	Quantile	$S_{2\times}$ 2022	$S_{2\times}$ 2025	Δ 2025–2022	Percentage change vs 2022
L_{Aeq}	Q25	9.876	9.725	−0.151	−1.5
L_{Aeq}	Q50	11.379	14.547	3.168	27.8
L_{Aeq}	Q75	12.843	19.054	6.211	48.4
N	Q25	17.263	23.458	6.195	35.9
N	Q50	20.923	28.162	7.239	34.6
N	Q75	24.742	32.533	7.791	31.5
SEL	Q25	7.355	6.848	−0.507	−6.9
SEL	Q50	8.405	11.711	3.306	39.3
SEL	Q75	9.406	16.376	6.970	74.1

Fundings

This work was supported by the Polish Ministry of Science and Higher Education (grant 0416/SBAD/0007).

Conflict of interest

The authors declare no conflict of interest.

Authors' contributions

Tomasz Nowakowski: conceptualization, methodology, supervision, formal analysis, calculations, and writing – original draft. Jacek Dwornik: investigation, 2022 measurement campaign, and writing – review and editing. Michał Strzelczyk: investigation, 2022 measurement campaign, signal time-window selection for both campaigns, and writing – review and editing. All authors reviewed and approved the final manuscript.

Use of AI tools

The authors declare that no generative AI or AI-assisted tools were used in the preparation of this manuscript.

Acknowledgments

The authors would like to thank the members of the Public Transport Engineering Student Research Group at Poznań University of Technology for their technical assistance during the field measurement campaign, conducted in accordance with the methodology specified by the authors.

References

1. American National Standards Institute (2025), *Measurement of sound pressure levels in air* (ANSI/ASA S1.13-2020 (R2025) Standard).
2. Andrés V.T., Martínez-Casas J., Denia F.D., Thompson D.J. (2022), Influence study of rail geometry and track properties on railway rolling noise, *Journal of Sound and Vibration*, **525**: 116701, https://doi.org/10.1016/j.jsv.2021.116701.
3. City of Poznań (2022), *Strategic noise map of the city of Poznań 2022 – report* [in Polish: *Strategiczna mapa hałasu miasta Poznania 2022 – raport*], Poznań, Poland.
4. Craven N.J., Kerry G. (2007), *A Good Practice Guide on the Sources and Magnitude of Uncertainty Arising in the Practical Measurement of Environmental Noise*, DTI Project: 2.2.1 - National Measurement System Programme for Acoustical Metrology, University of Salford.

5. European Standard (2019), *Railway applications – noise emission – rail and wheel roughness measurement related to rolling noise generation* (EN 15610:2019 Standard).
6. International Association of Public Transport (UITP) (2019), *Public transport: moving Europe forward 2014–2019*, Brussels.
7. International Organization for Standardization (2013), *Railway applications – acoustics – measurement of noise emitted by railbound vehicles*, International Organization for Standardization (ISO Standard No. 3095:2013), https://www.iso.org/standard/55726.html.
8. International Organization for Standardization (2017), *Acoustics – Methods for calculating loudness – part 1: Zwicker method* (ISO Standard No. 532-1:2017), https://www.iso.org/standard/63077.html.
9. Joint Committee for Guides in Metrology (JCGM) (2008), *Evaluation of measurement data – guide to the expression of uncertainty in measurement*.
10. Jones C.J.C., Thompson D.J., Diehl R.J. (2006), The use of decay rates to analyse the performance of railway track in rolling noise generation, *Journal of Sound and Vibration*, **293**(3–5): 485–495, https://doi.org/10.1016/j.jsv.2005.08.060.
11. Kryter K.D. (1962), Methods for the calculation and use of the articulation index, *The Journal of the Acoustical Society of America*, **34**(11): 1689–1697, https://doi.org/10.1121/1.1909094.
12. Lakušić S., Dragčević V., Rukavina T. (2005), The impact of tram track fastening systems on noise level, *WIT Transactions on The Built Environment*, **77**: 487–497, https://doi.org/10.2495/UT050471.
13. Nowakowski T., Firlik B., Staśkiewicz T. (2019), Developing assumptions for the tram noise attenuation passive system using the noise maps analysis method, *Archives of Acoustics*, **44**(4): 783–792, https://doi.org/10.24425/aoa.2019.129733.
14. Nowakowski T., Komorski P. (2024), Tram noise annoyance: the role of different psychoacoustic measures in the assessment of noise, *Applied Acoustics*, **219**: 109946, https://doi.org/10.1016/j.apacoust.2024.109946.
15. OpenAerialMap (n.d.), *OpenAerialMap viewer*, https://map.openaerialmap.org/ (access: 20.05.2026).
16. Remington P.J. (1976), Wheel/rail noise – part IV: rolling noise, *Journal of Sound and Vibration*, **46**(3): 419–436, https://doi.org/10.1016/0022-460X(76)90864-6.
17. Sun W., Thompson D., Toward M., Wiseman M., Ntotsios E., Byrne S. (2020), The influence of track design on the rolling noise from trams, *Applied Acoustics*, **170**: 107536, https://doi.org/10.1016/j.apacoust.2020.107536.
18. Terhardt E., Stoll G., Seewann M. (1982), Algorithm for extraction of pitch and pitch salience from complex tonal signals, *The Journal of the Acoustical Society of America*, **71**(3): 679–688, https://doi.org/10.1121/1.387544.
19. Tetsuya H., Yano T., Murakami Y. (2017), Annoyance due to railway noise before and after the opening of the Kyushu Shinkansen Line, *Applied Acoustics*, **115**: 173–180, https://doi.org/10.1016/j.apacoust.2016.09.004.
20. Thompson D.J. (2009), *Railway Noise and Vibration: Mechanisms, Modelling and Means of Control*, 1st ed., Elsevier, Oxford.
21. Thompson D.J., Jones C.J.C. (2000), A review of the modelling of wheel/rail noise generation, *Journal of Sound and Vibration*, **231**(3): 519–536, https://doi.org/10.1006/jsvi.1999.2542.
22. Vincent N., Bouvet P., Thompson D.J., Gautier P.E. (1996), Theoretical optimization of track components to reduce rolling noise, *Journal of Sound and Vibration*, **193**(1): 161–171, https://doi.org/10.1006/jsvi.1996.0255.
23. Zhang X., Hou X., Thompson D., Li Q., Zhu J. (2026), A method of economic evaluation of noise mitigation measures in urban rail transit, *International Journal of Transportation Science and Technology*, https://doi.org/10.1016/j.ijtst.2025.08.006.